nature cell biology

p53 regulates biosynthesis through direct inactivation of glucose-6-phosphate dehydrogenase

Peng Jiang[1,2,4], Wenjing Du[1,2,4], Xingwu Wang[1], Anthony Mancuso[2], Xiang Gao[3], Mian Wu[1,5] and Xiaolu Yang[2,5]

Cancer cells consume large quantities of glucose and primarily use glycolysis for ATP production, even in the presence of adequate oxygen[1,2]. This metabolic signature (aerobic glycolysis or the Warburg effect) enables cancer cells to direct glucose to biosynthesis, supporting their rapid growth and proliferation[3,4]. However, both causes of the Warburg effect and its connection to biosynthesis are not well understood. Here we show that the tumour suppressor *p53*, the most frequently mutated gene in human tumours, inhibits the pentose phosphate pathway[5] (PPP). Through the PPP, p53 suppresses glucose consumption, NADPH production and biosynthesis. The p53 protein binds to glucose-6-phosphate dehydrogenase (G6PD), the first and rate-limiting enzyme of the PPP, and prevents the formation of the active dimer. Tumour-associated p53 mutants lack the G6PD-inhibitory activity. Therefore, enhanced PPP glucose flux due to p53 inactivation may increase glucose consumption and direct glucose towards biosynthesis in tumour cells.

The tumour suppressor p53 invokes anti-proliferative processes, of which the best understood include cell cycle arrest, DNA repair and apoptosis[6,7]. Recent studies indicated that p53 also has a role in modulating metabolism including glycolysis and oxidative phosphorylation[8–10]. However, the role of p53 in regulating biosynthesis is less well understood. The PPP is important for both glucose catabolism and biosynthesis[5]. In an oxidative phase, the PPP generates NADPH (nicotinamide adenine dinucleotide phosphate, reduced), the principal intracellular reductant required for reductive biosynthesis such as the synthesis of lipid, and ribose 5-phosphate, an essential precursor for biosynthesis of nucleotides. This is followed by a non-oxidative interconversion of ribose 5-phosphate to the intermediates in the glycolytic pathways. Despite the vital role of the PPP in biosynthesis and its close link to glycolysis, the regulation of the PPP in tumour cells remains unclear.

To investigate whether p53 modulates the PPP, we compared the oxidative PPP flux in isogenic $p53^{+/+}$ and $p53^{-/-}$ human colon cancer HCT116 cells[11]. Cells were cultured in medium containing [2-^{13}C]glucose, and the glucose metabolites were measured by nuclear magnetic resonance (NMR) spectroscopy. As shown in Fig. 1a, the absence of p53 resulted in a strong enhancement (~50%) in oxidative PPP flux, indicating that p53 suppresses the PPP. The absence of p53 concomitantly led to a strong increase in glucose consumption, and this was observed in both HCT116 and mouse embryonic fibroblast (MEF) cells (Fig. 1b,c). Inhibition of G6PD using either small interfering RNA (siRNA) or dehydroepiandrosterone (DHEA) reversed the increase in glucose consumption caused by p53 deficiency, but had little effect on glucose consumption in $p53^{+/+}$ cells (Fig. 1b,c). These results indicate that p53 deficiency increases glucose consumption mainly through an enhanced PPP flux.

The lack of p53 also correlated with elevated lactate production (Fig. 1d,e). However, inhibition of G6PD in these cells increased, rather than decreased, lactate production, regardless of p53 status. Therefore, glucose flux through the PPP may itself lower lactate production. The suppression of lactate production may be related to the ability of p53 to decrease glycolysis[8] or increase oxidative phosphorylation[9].

The PPP plays a significant role in the production of cellular NADPH. The lack of p53 led to a strong increase in the NADPH level in HCT116 cells (~2-fold, Fig. 2a). Similarly, knocking down p53 in U2OS cells with small hairpin RNA (shRNA) strongly increased NADPH levels (Supplementary Fig. S1a). Treatment with *G6PD* siRNA minimized the difference in NADPH levels between p53-proficient and -deficient cells. To verify the cell culture findings in animals, we compared the NADPH levels in various tissues from $p53^{-/-}$ and $p53^{+/+}$ mice. The tissues from $p53^{-/-}$ mice—including heart, liver, kidney and lung—exhibited substantially

[1]Hefei National Laboratory for Physical Sciences at Microscale and School of Life Sciences, University of Science and Technology of China, Hefei, Anhui, 230027, China. [2]Department of Cancer Biology and Abramson Family Cancer Research Institute, University of Pennsylvania School of Medicine, Philadelphia, Pennsylvania 19096, USA. [3]Model Animal Research Center, State Key Laboratory of Pharmaceutical Biotechnology, Nanjing University, Nanjing 210093, China. [4]These authors contributed equally to this work.
[5]Correspondence should be addressed to M.W. or X.Y. (e-mail: wumian@ustc.edu.cn or xyang@mail.med.upenn.edu)

Received 8 November 2010; accepted 25 November 2010; published online 20 February 2011; DOI: 10.1038/ncb2172

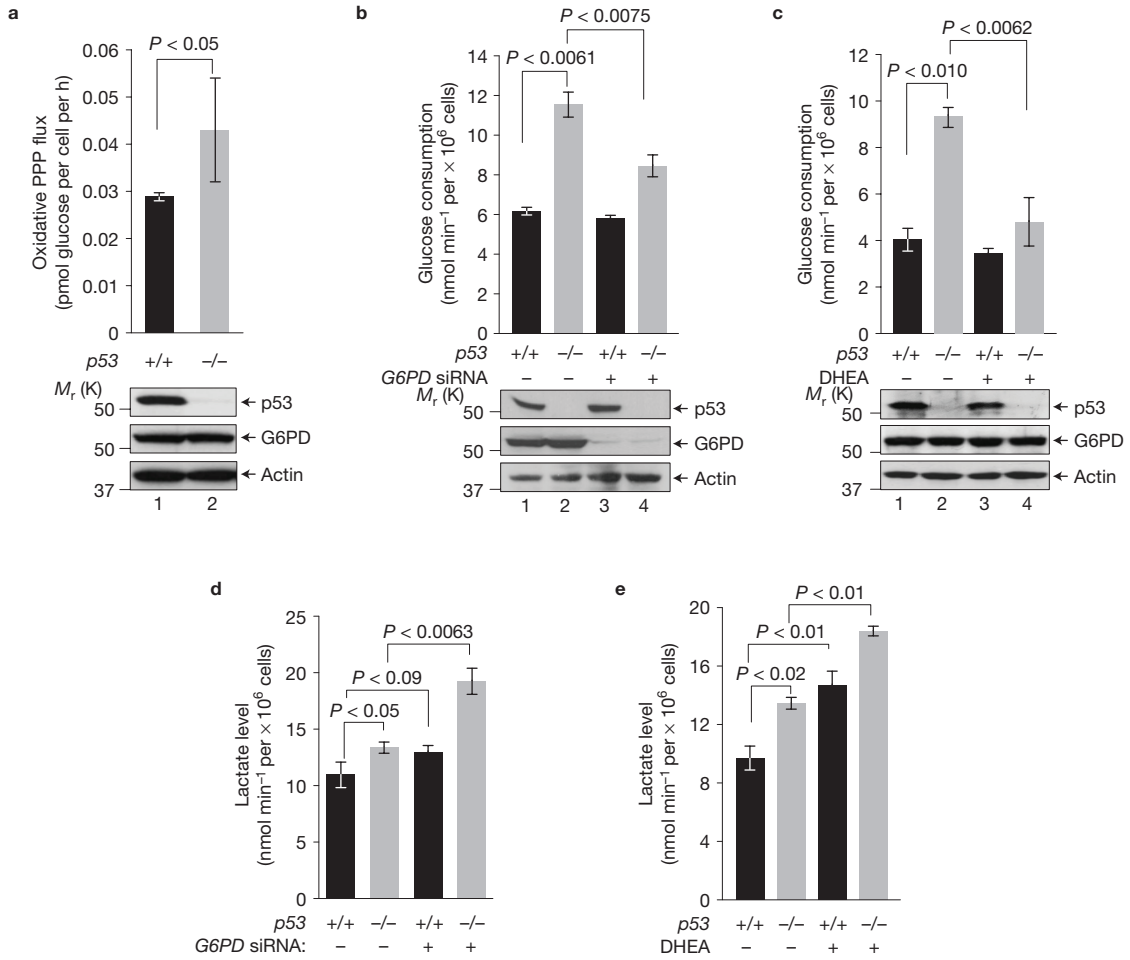

Figure 1 p53 deficiency correlates with increases in PPP flux, glucose consumption and lactate production. (**a**) $p53^{+/+}$ and $p53^{-/-}$ HCT116 cells were cultured in medium containing [2-^{13}C]glucose. Oxidative PPP flux (top) was measured based on the rate of glucose consumption and the ratio of ^{13}C incorporated into carbon 2 (indicating glycolysis) and carbon 3 (indicating PPP) of lactate by NMR spectroscopy. Data are means ± s.d. ($n = 3$). Protein expression is shown at the bottom, with molecular weight standards indicated on the left. (**b**) $p53^{+/+}$ and $p53^{-/-}$ HCT116 cells were treated with *G6PD* siRNA and control siRNA (–). Top: glucose consumption. Data are means ± s.d. ($n = 3$). Bottom: the expression of p53, G6PD and actin (a loading control). (**c**) $p53^{+/+}$ and $p53^{-/-}$ MEF cells were treated with 1 mM DHEA or vehicle (–) for 24 h. Top: glucose consumption. Data are means ± s.d. ($n = 3$). Bottom: protein expression (**d**,**e**). Lactate levels in cells from **b** (**d**) and **c** (**e**). Data are means ± s.d. ($n = 3$ for each panel).

elevated NADPH levels, compared with those in the corresponding tissues from $p53^{+/+}$ mice (Fig. 2b). The exception was found in the spleen. In this tissue, the activity of G6PD was very low (Fig. 2g), and the PPP might not contribute substantially to the overall NADPH production. In contrast to p53 downregulation, overexpression of p53 led to a strong decrease in NADPH levels (Supplementary Fig. S1b).

NADPH is required for the biosynthesis of lipid. To assess the effect of p53 on lipid accumulation, we treated $p53^{+/+}$ and $p53^{-/-}$ MEF cells with a combination of insulin, rosiglitazone, dexamethasone and isobutylmethylxanthine, which stimulates lipogenesis[12]. The $p53^{-/-}$ MEF cells showed enhanced lipid levels, compared with $p53^{+/+}$ MEF cells, as evaluated by Oil Red O staining (Fig. 2c). The lack of p53 also resulted in higher levels of lipid in HCT116 cells (Supplementary Fig. S1c). The difference in lipid accumulation between $p53^{+/+}$ and $p53^{-/-}$ cells diminished on treatment with *G6PD* siRNA or DHEA. We also evaluated the effect of p53 on the formation of fat droplets in the liver. The liver of $p53^{-/-}$ mice had a larger number of bigger fat droplets, compared with the liver of $p53^{+/+}$ mice (Fig. 2d). Together, these results indicate that p53 inhibits NADPH production and lipid accumulation by lowering the glucose flux through the PPP.

To investigate the mechanism by which p53 regulates the PPP, we assayed the activity of G6PD, a key regulatory point of the PPP. The lack of p53 correlated with a strong elevation in G6PD activity in both MEF and HCT116 cells (Fig. 2e and Supplementary Fig. S1d,e). Similarly, when p53 was knocked down in U2OS cells with shRNA, G6PD activity nearly doubled (Fig. 2f). Furthermore, in mice tissues where G6PD activity could be adequately detected (for example liver, lung and kidney), the lack of p53 was associated with highly elevated G6PD activity (Fig. 2g). Conversely, overexpression of wild-type p53 in the p53-deficient cell lines (H1299 and $p53^{-/-}Mdm2^{-/-}$ MEF) caused a noticeable decrease in G6PD activity (Supplementary Fig. S1f,g). These results show that p53 suppresses G6PD activity.

In each of the cell lines and tissues that were examined, the levels of the G6PD protein remained unchanged when p53 was downregulated or overexpressed (Fig. 2a,b,f and Supplementary Fig. S1). Moreover, p53 did not change the level of G6PD transcript (Fig. 3a). To rule out the involvement of other p53 target genes in the inhibition of G6PD,

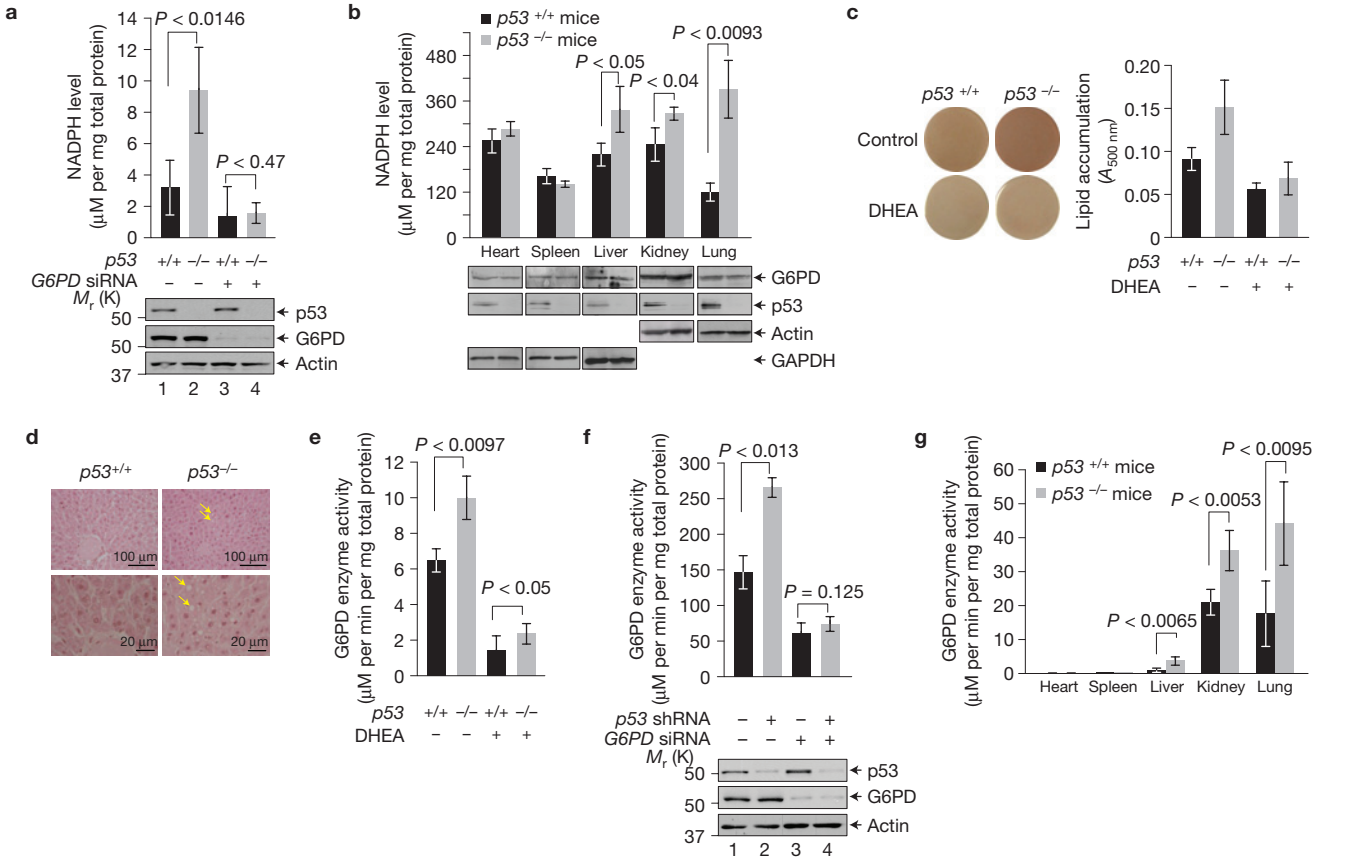

Figure 2 p53 regulates NADPH levels, lipid accumulation and G6PD activity. (**a**) NADPH levels (means ± s.d., $n = 3$) in $p53^{+/+}$ and $p53^{-/-}$ HCT116 cells treated with *G6PD* siRNA or control siRNA. Protein expression is shown below. (**b**) NADPH levels (means ± s.d., $n = 3$) in tissues from $p53^{+/+}$ and $p53^{-/-}$ mice maintained on a normal diet. Protein expression is shown below. (**c**) $p53^{+/+}$ and $p53^{-/-}$ MEF cells treated with or without DHEA were cultured in the presence of insulin, rosiglitazone, isobutylmethylxanthine and dexamethasone. Lipid contents were analysed by Oil Red O staining. Left: Oil Red O-stained dishes. Right: staining was quantified by absorbance at 500 nm. Data are means ± s.d. ($n = 3$). (**d**) Histological sections of liver tissue from $p53^{+/+}$ and $p53^{-/-}$ mice were stained with haematoxylin and eosin. Arrows indicate fat droplets. (**e**) G6PD activity (means ± s.d., $n = 3$) in $p53^{+/+}$ and $p53^{-/-}$ MEF cells treated with or without DHEA. (**f**) U2OS cells stably expressing *p53* shRNA or control shRNA (−) were transfected with *G6PD* siRNA or control siRNA (−). G6PD activity (top) and protein expression (bottom) were analysed. Data are means ± s.d. ($n = 3$). (**g**) G6PD activity in tissues from $p53^{-/-}$ and $p53^{+/+}$ mice maintained on a normal diet. G6PD activity is the mean ± s.d. of three $p53^{+/+}$ or four $p53^{-/-}$ mice.

we used an inhibitor of p53 transcriptional activity, pifithrin-α (PFTα; ref. 13). PFTα impeded p53-induced expression of p21, but did not restore p53-inhibited G6PD activity (Fig. 3b and Supplementary Fig. S2a). We also used the protein synthesis inhibitor cycloheximide, alone or together with the DNA damaging agent doxorubicin. Treatment of $p53^{+/+}$ HCT116 cells with cycloheximide alone resulted in a lower level of p53, which was accompanied by a higher activity of G6PD (Fig. 3c). Simultaneous treatment with cycloheximide and doxorubicin led to a stabilization of p53 above the basal level in unstressed cells, and a concurrent drop of G6PD activity below its basal level (Fig. 3c). As controls, none of these treatments altered G6PD activity in $p53^{-/-}$ HCT116 cells. In addition, the p53 mutant V122A, which has a transactivation activity comparable to or even higher than wild-type p53 dependent on the target gene[14], failed to inhibit G6PD (Supplementary Fig. S2b). Moreover, we treated cells with the nuclear export inhibitor leptomycin B to prevent cytoplasmic accumulation of p53 (refs 15,16). Leptomycin B reversed p53-mediated inhibition of G6PD (Supplementary Fig. S2c–e). Together, these results show that inhibition of G6PD by p53 is independent of transcription or translation and is a cytoplasmic, not nuclear, function of p53.

We next investigated whether p53 interacts with G6PD. Flag-tagged p53 specifically associated with enhanced green fluorescent protein (eGFP)–G6PD *in vivo* (Fig. 3d). Similarly, endogenous p53 interacted with endogenous G6PD (Fig. 3e). G6PD is a cytoplasmic protein, whereas p53 is present in both the cytoplasm and the nucleus, and consistently, the p53–G6PD interaction occurred in the cytoplasm (Supplementary Fig. S2f–h). This interaction was enhanced when cells were treated with the proteasome inhibitor MG132 doxorubicin, both of which stabilized p53 (Fig. 3d,e and Supplementary Fig. S2h). The binding between p53 and G6PD is direct, as shown by a pulldown assay with purified recombinant proteins (Fig. 3f). Analysis of the p53–G6PD binding in real time using surface plasmon resonance (BIAcore) showed that the dissociation constant (K_d) of p53 from G6PD was 173 ± 50 nM (Fig. 3g). G6PD is a highly conserved protein, and human p53 interacted with G6PD proteins from both the bacterium *Leuconostoc mesenteroides* and the yeast *Saccharomyces cerevisiae* (Supplementary Fig. S3a–c).

Consistent with their direct interaction, purified wild-type p53 could inhibit purified G6PD *in vitro* (Fig. 4a,b). In addition, introducing p53 into two *S. cerevisiae* strains, AH109 and EGY48, led to more

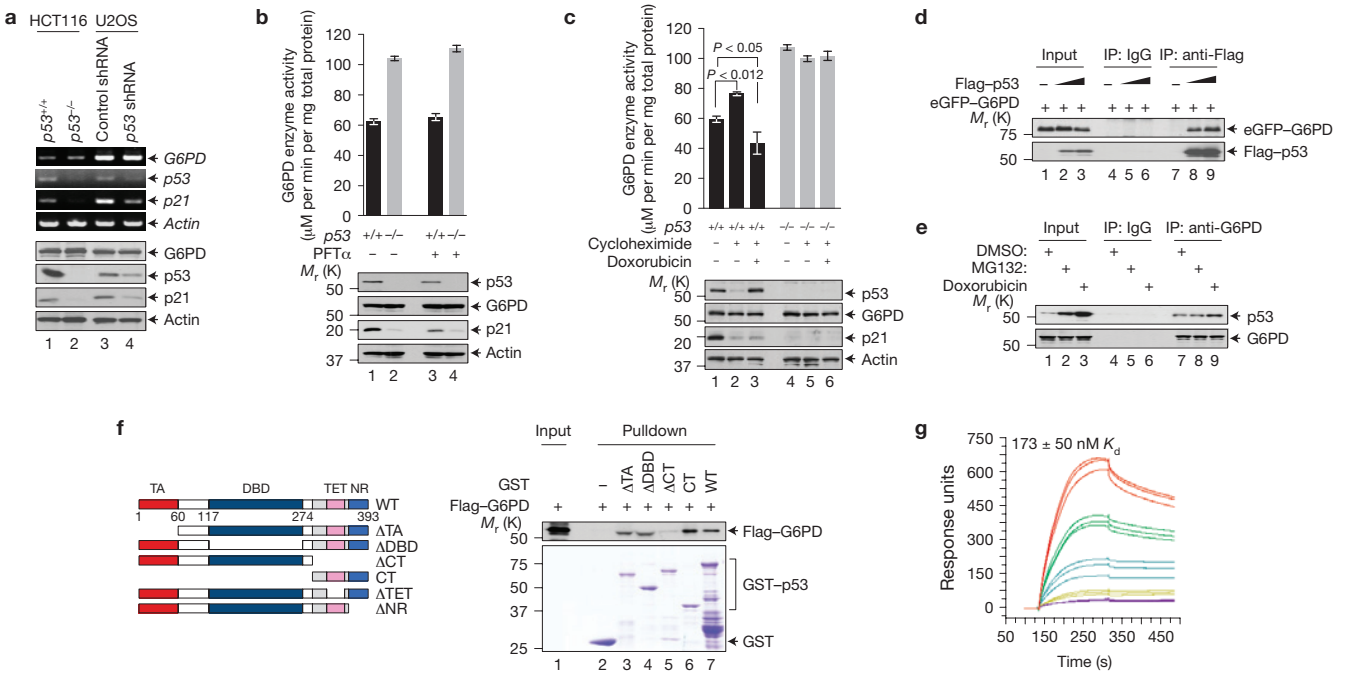

Figure 3 p53 interacts with G6PD and inhibits its activity independently of transcription. (**a**) $p53^{+/+}$ and $p53^{-/-}$ HCT116 cells, and U2OS cells transfected with *p53* shRNA and control shRNA, were analysed by PCR with reverse transcription (top) and western blot (bottom). (**b**,**c**) $p53^{+/+}$ and $p53^{-/-}$ HCT116 cells were treated with or without 20 μM of PFTα for 24 h (**b**), or treated with or without doxorubicin (2 μM) for 1 h, and then with or without cycloheximide (20 μM) for 2 h (**c**). Cells were analysed for G6PD activity (top) and protein expression (bottom). Data are means ± s.d. ($n = 3$). (**d**) H1299 cells were transfected with eGFP–G6PD alone or together with increasing amounts of Flag–p53. Cell lysates were immunoprecipitated with an anti-Flag antibody and an isotype-matching control antibody (IgG). Immunoprecipitated proteins (IP) and 5% input were analysed by western blot. (**e**) $p53^{+/+}$ HCT116 cells were treated with MG132 (20 μM), doxorubicin (2 μM) or vehicle (dimethylsulphoxide). Cell lysates were incubated with anti-G6PD antibody or a control antibody (IgG). Immunoprecipitates and input were analysed by western blot. (**f**) Left, schematic representation of p53 and its deletion mutants. WT, wild-type; TA, transactivation domain; DBD, DNA-binding domain; CT, C-terminal region; TET, tetramerization domain; NR, negative regulation domain. The amino acids at the domain boundaries are indicated. Right, purified GST and GST fusions of wild-type and mutant p53 proteins were incubated separately with recombinant Flag–G6PD protein conjugated to beads. Beads-bound and input proteins were analysed by western blot using anti-Flag (top) and Coomassie blue staining (bottom). (**g**) The dissociation constant (K_d) for p53 from immobilized G6PD was determined by surface plasmon resonance (BIAcore). A real-time graph of response units against time is shown. The on rate was $7.53 \pm 1.59 \times 10^3\ M^{-1}\ s^{-1}$, and the off rate was $1.30 \pm 0.03 \times 10^{-3}\ s^{-1}$.

than 60% inhibition of G6PD activity (Supplementary Fig. S3d,e). Expression of p53 also strongly reduced G6PD activity in *Escherichia coli* (Supplementary Fig. S3f,g).

To delineate the structural determinants for the inhibitory activity of p53 towards G6PD, we used a panel of p53 deletion mutants. The G6PD interaction domain was mapped to the carboxy-terminal region of p53 (Fig. 3f and Supplementary Fig. S3b,c). However, the C-terminal region alone was not sufficient for G6PD inhibition; the transactivation (TA) and DNA-binding domain (DBD) were also required (Fig. 4a,b and Supplementary Fig. S1f). A further deletion analysis showed that within the C-terminal region, the negative regulatory (NR) domain, but not the tetramerization (TET) domain, was required for interaction with and inhibition of G6PD (Supplementary Fig. S4a,b).

The involvement of multiple domains of p53 in G6PD inhibition led us to test tumour-associated p53 mutants, most of which harbour missense mutations. Unlike wild-type p53, three p53 mutants (R175H, R273H and G279E) showed minimal or no activity in inhibiting G6PD (Fig. 4c and Supplementary Figs S1g, S2b, S3g), even though at least two of them (R175H and R273H) retained the ability to bind to G6PD (Supplementary Fig. S4c). Another tumour-associated, temperature-sensitive mutant (A138V) inhibited G6PD activity at the permissive temperature 32 °C, but not at the non-permissive temperature 37 °C. Moreover, the inhibitory effect at 32 °C was abolished with the introduction of R273H (Supplementary Fig. S4d). To examine the effect of p53 mutants that are expressed at endogenous levels, we used a panel of SW480 cells, in which the endogenous p53 mutant (R273H/P309S) can be inducibly knocked down and, at the same time, exogenous p53 mutants containing either G245S or R248W, alone or in combination with alterations in activation domain 1 or 2, were inducibly expressed at levels comparable to the endogenous p53 mutant[17]. Replacement of the endogenous mutant p53 with exogenous mutants caused little or no changes in G6PD activity (Supplementary Fig. S4e). In contrast, a p53 mutant with increased thermodynamic stability[18] (N239Y), exhibited enhanced ability to inhibit G6PD (Fig. 4d). As tumour-associated mutations impair the native conformation of p53 and the N239Y mutation stabilizes it, the inhibition on G6PD is probably attributed to the native conformation of p53.

We investigated how p53 inhibits G6PD activity. G6PD is in equilibrium of inactive monomer and active dimer[19,20]. In both HCT116 and MEF cells, the lack of p53 led to a strong increase in G6PD dimer and a corresponding decrease in G6PD monomer (Fig. 4e). In a transfection assay, p53 reduced the interaction of two differentially tagged G6PD proteins (Flag–G6PD

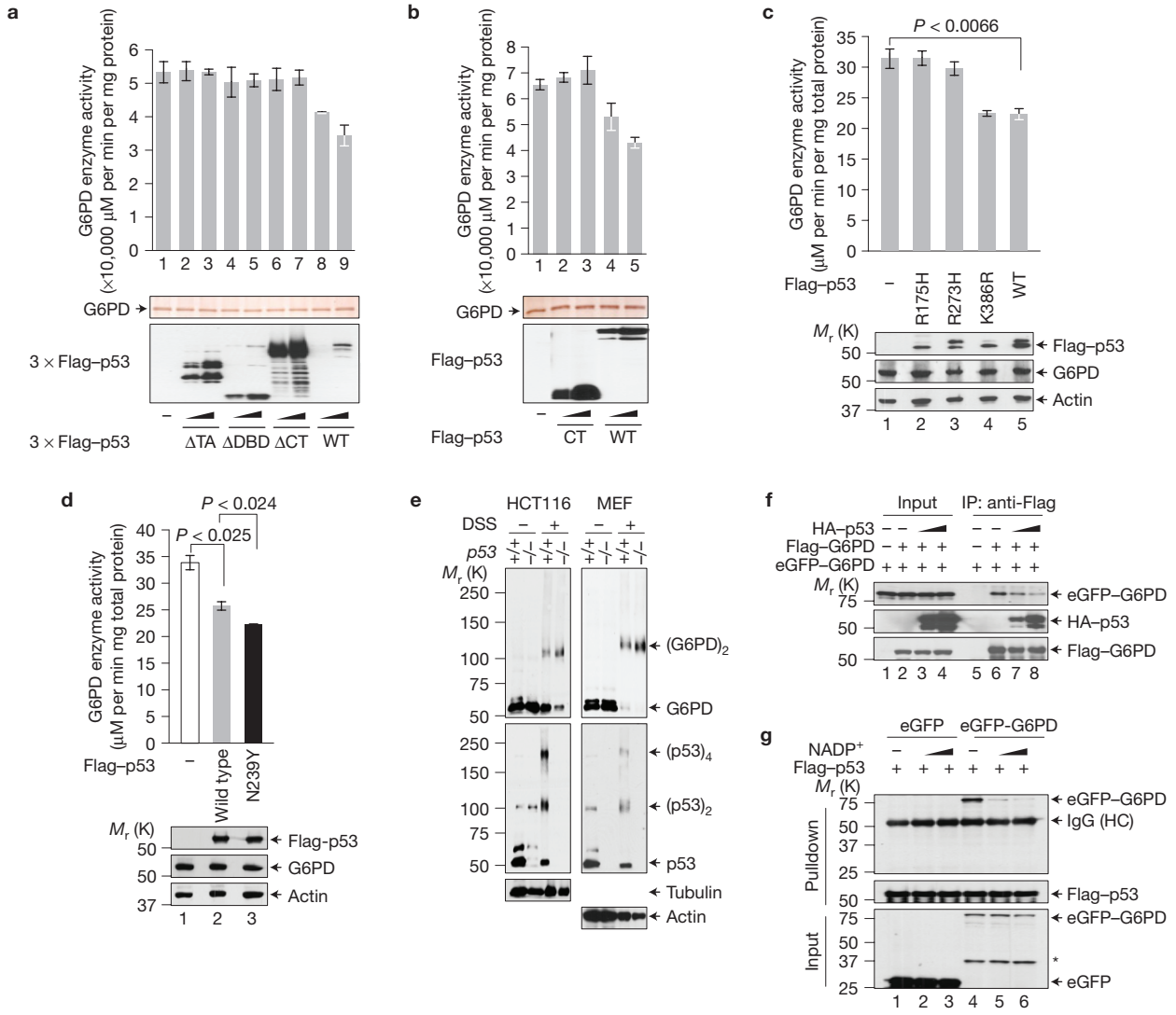

Figure 4 p53 inhibits the formation of dimeric G6PD holoenzyme. (**a**,**b**) Activity of the G6PD protein after being incubated with increasing amounts of purified wild-type or mutant p53 proteins (top). Proteins were analysed by silver staining (middle) and anti-Flag western blot (bottom). The p53 proteins were tagged with either three copies (**a**) or one copy (**b**) of the Flag epitope. Data are means ± s.d. ($n = 3$). (**c**,**d**) H1299 cells (**c**) and $p53^{-/-}Mdm2^{-/-}$ MEF cells (**d**) were transfected separately with wild-type and mutant p53 proteins as indicated. G6PD activity (top) and protein expression (bottom) were analysed. The K386R mutation blocks p53 SUMOylation. Data are means ± s.d. ($n = 3$). (**e**) Extracts of $p53^{+/+}$ and $p53^{-/-}$ HCT116 and MEF cells were treated with and without 5 mM disuccinimidyl suberate (DSS) and analysed by western blot with antibodies against G6PD and p53, and as controls, tubulin and actin. The positions of various forms of G6PD and p53 are indicated. (**f**) H1299 cells were transfected with Flag–G6PD, eGFP–G6PD and different amounts of haemagglutinin (HA)–p53. Cell lysates were incubated with anti-Flag antibody. Input and immunoprecipitates were analysed by western blot. (**g**) Lysates from $p53^{-/-}Mdm2^{-/-}$ MEF cells expressing eGFP or eGFP–G6PD were incubated with Flag–p53 immobilized on M2 beads or control beads in the presence of increasing amounts of $NADP^+$ (0, 0.1 and 1 mM). Input and beads-bound (pulldown) proteins were analysed by western blot. HC, IgG heavy chain; asterisk, non-specific band.

and eGFP–G6PD) in a dose-dependent manner (Fig. 4f). G6PD requires its substrate nicotinamide adenine dinucleotide phosphate ($NADP^+$) as the cofactor for the formation of holoenzyme, a property that ensures higher G6PD activity and thus more NADPH production when the NADPH/$NADP^+$ ratio drops[5]. $NADP^+$ diminished the interaction between G6PD and p53 in a dose-dependent manner (Fig. 4g), indicating that the binding of p53 to G6PD is incompatible with the binding of $NADP^+$ to G6PD. These results indicate that p53 may disrupt the formation of the dimeric G6PD holoenzyme.

The levels of p53 are kept low in unstressed cells owing to its rapid degradation in the proteasome. A semi-quantitative western blot assay showed the levels of cytoplasmic p53 were approximately 3% that of G6PD. The levels of p53 increased to ~10% that of G6PD when p53 was stabilized by either MG132 or doxorubicin (Supplementary Fig. S5a). Accordingly, most p53 molecules bound to G6PD in unstressed cells, but a small percentage of G6PD bound to p53, as shown by immunodepletion assays (Fig. 5a,b). Only when p53 was stabilized by MG132 and doxorubicin did a significant portion of p53 molecules become separated from G6PD (Fig. 5b).

The discrepancy between the amounts of p53 that stably bind to G6PD and the strong effect of p53 on overall G6PD activity raises the possibility that p53 is capable of inhibiting G6PD activity through

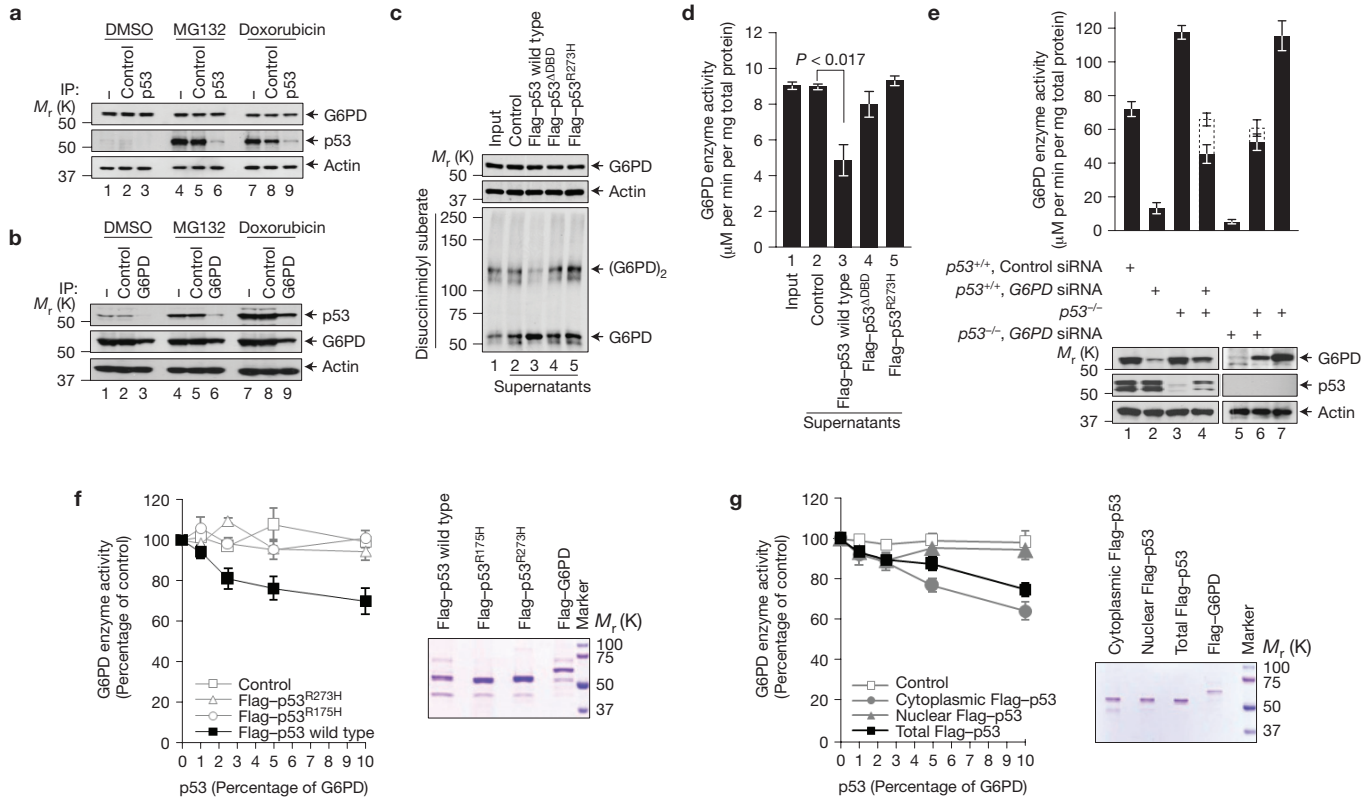

Figure 5 p53 suppresses G6PD through transient interaction and at substoichiometric ratios. (**a**,**b**) $p53^{+/+}$ HCT116 cells were treated with dimethylsulphoxide, MG132 and doxorubicin. The cytosolic fraction was immunoprecipitated separately with a control antibody and anti-p53 (**a**) or G6PD (**b**) antibody, plus protein A/G beads. The lysates before (−) and after immunoprecipitation were analysed by western blot. (**c**,**d**) Lysates from $p53^{-/-}$ MEF cells were first incubated with Flag-tagged p53 proteins immobilized on beads and control beads, and then were separated from the beads. (**c**) Levels of proteins (top and middle) and G6PD dimerization (bottom) in the input lysates (Input) and supernatant after being incubated with the beads. (**d**) G6PD activity in the input lysates and supernatants. Data in **d** are means ± s.d. ($n = 3$). (**e**) $p53^{+/+}$ and $p53^{-/-}$ HCT116 cells were either treated separately with *G6PD* siRNA and control siRNA, or untreated. Filled columns, actual G6PD activity in the 1:1 mixtures of the indicated lysates (lanes 4 and 6) and in individual lysates (the other lanes). Dashed columns, expected G6PD activity in mixtures based on the averages of the individual lysates. Protein expression is shown at the bottom. The samples were derived from the same conditions. Data are means ± s.d. ($n = 3$). (**f**,**g**) Left, activity of G6PD after being incubated with total wild-type and mutant p53 proteins (**f**) or cytosolic, nuclear and total wild-type p53 (**g**). p53 proteins were used at molar ratios of 1, 2.5, 5 and 10% that of G6PD. Data are means ± s.d. ($n = 3$). Right, Coomassie blue staining of purified proteins.

transient interaction and at substoichiometric ratios. To test whether p53 can inhibit G6PD through transient interaction, we incubated lysates of $p53^{-/-}$ MEF cells with recombinant p53 immobilized on beads and then separated the lysates from the beads. The treated lysates contained virtually all of the G6PD protein and undetectable amounts of p53 (Fig. 5c and Supplementary Fig. S5b), but showed much reduced G6PD activity (~50%) and low levels of G6PD dimer (Fig. 5c,d). In the same experiment, unconjugated control beads and beads conjugated with $p53^{\Delta DBD}$ or $p53^{R273H}$ protein all failed to inhibit G6PD activity and G6PD dimerization.

To assess whether one p53 molecule can inhibit multiple G6PD molecules, we first mixed extracts of $p53^{+/+}$ HCT116 cells treated with *G6PD* siRNA (with low G6PD, but normal p53 level) with extracts of $p53^{-/-}$ HCT116 cells (with normal G6PD level, but no p53). The G6PD activity in the mix was substantially lower than the calculated average of these two extracts (Fig. 5e, column 4), indicating that the small amounts of p53 protein in the former extracts could significantly inhibit the activity of a much larger amount of G6PD in the latter extracts. In a control experiment, when $p53^{+/+}$ HCT116 extracts were replaced with $p53^{-/-}$ HCT116 extracts that were used, the G6PD activity in the mix was approximately the average of the two extracts that were used, as expected (Fig. 5e, column 6).

We next mixed purified recombinant proteins at low molar ratios of p53 versus G6PD. At a ratio of 2.5% (approximately the ratio of these proteins in unstressed cells; Supplementary Fig. S5a), p53 decreased G6PD activity by 20% (Fig. 5f), indicating that one p53 molecule could inactivate up to eight G6PD molecules. This was probably an underestimate, because of the lability of p53 protein. The inhibition efficiency decreased at higher ratios of p53 versus G6PD, but increased at a lower molar ratio (Fig. 5f). In contrast, R273H and R175H mutants failed to inhibit G6PD at any ratio examined (Fig. 5f). Together, these results indicate that wild-type p53 may act as a catalyst to inactivate G6PD.

To evaluate cytoplasmic and nuclear pools of p53 in the inhibition of G6PD, we purified p53 proteins from these cellular compartments. Cytoplasmic p53 exhibited robust inhibitory activity towards G6PD. However, nuclear p53 protein showed minimal activity (Fig. 5g). In the cell lysates, cytoplasmic p53 was mainly in monomeric form, whereas nuclear p53 was mostly in tetrameric form (Supplementary Fig. S5c). This difference

remained even after these proteins were purified and adjusted to the same concentration (Supplementary Fig. S5d). Therefore, the cytoplasmic and nuclear p53 proteins seem to be intrinsically different in their oligomerization status and their ability to inhibit G6PD.

This study identifies an important role for p53 in regulating G6PD. Through this regulation, p53 exerts a powerful surveillance on the metabolic pathways that are critical for both glucose catabolism and biosynthesis. The suppression of G6PD by p53 is evident in unstressed cells and is independent of transcription. As most cytoplasmic p53 associates with G6PD in unstressed cells (Fig. 5a,b), inhibiting G6PD is probably a main function of cytoplasmic p53 in these cells. In stressed cells where p53 is stabilized, a portion of cytoplasmic p53 becomes free of G6PD and may carry out other functions previously attributed to cytoplasmic p53, such as the interaction with B-cell lymphoma 2 (Bcl-2) family proteins[21]. Notably, p53 can inhibit G6PD through transient interactions and at levels much lower than that of G6PD, indicating that p53 may act as a catalyst to induce conformational changes in G6PD. This function is attributed to the entire p53 protein, perhaps with the exception of the tetramerization domain, and seems to be specific to the p53 proteins originating from the cytoplasm, but not the nucleus. Metabolism is known to be controlled by allosteric interactions, covalent modifications of enzymes, and changes in their amounts. p53-induced conformational conversion of G6PD may represent a previously unknown mechanism of metabolic regulation. p53-mediated inhibition of the PPP probably dominates the effect of *TIGAR* (tumour protein 53 (TP53)-induced glycolysis and apoptosis regulator), a previously identified p53 target gene that stimulates the PPP (ref. 22); this is shown by the enhanced PPP flux and NADPH production in p53-deficient cells. Given the importance of p53 in suppressing the PPP, the prevalent inactivation of p53 in tumour cells probably accelerates glucose consumption, and, at the same time, directs glucose for rapid production of macromolecules by means of an increase in the PPP flux. Therefore, p53 inactivation not only contributes to the Warburg effect, but also links it to enhanced biosynthesis. □

METHODS

Methods and any associated references are available in the online version of the paper at http://www.nature.com/naturecellbiology/

Note: Supplementary Information is available on the Nature Cell Biology website

ACKNOWLEDGEMENTS

We thank W. Xie for isolating $p53^{+/+}$ and $p53^{-/-}$ MEF cells; X. Chen for SW480 cells; B. Vogelstein and W. El-Deiry for HCT116 cells; J. Cross, N. Li, J. Wu, Y. Mei, A. Stonestrom, W. Tan, H. Liu, Y. Hao, X. Zhao and Z. Lou for technical assistance; C. B. Thompson and J. Delikatny for helpful comments; and A. Stonestrom and E. Thompson for help with manuscript preparation. Supported by grants from the China National Natural Science Foundation (31030046), the Ministry of Science and Technology (2010CB912804 and 2011CB966302) and the Chinese Academy of Sciences (KSCX1-YW-R-57) to M.W. and the US National Institutes of Health (CA088868 and GM060911) and the Department of Defense (W81XWH-07-1-0336 and W81XWH-10-1-0468) to X.Y.

AUTHOR CONTRIBUTIONS

P.J., W.D., M.W. and X.Y. designed the experiments and interpreted results. P.J. and W.D. carried out all the experiments, except those mentioned below. X.W. carried out the experiments on G6PD activity in yeast, the surface plasmon resonance, and lipid droplets in mouse liver. A.M. and P.J. analysed the oxidative PPP flux. X.G. supplied the p53 wild-type and knockout mice. X.Y. wrote the manuscript with the help of P.J. and W.D.

COMPETING FINANCIAL INTERESTS

The authors declare no competing financial interests.

Published online at http://www.nature.com/naturecellbiology
Reprints and permissions information is available online at http://npg.nature.com/reprintsandpermissions/

1. Warburg, O., Posener, K. & Negelein, E. Ueber den Stoffwechsel der Tumoren. *Biochem. Z.* **152,** 319–344 (1924).
2. Warburg, O. On the origin of cancer cells. *Science* **123,** 309–314 (1956).
3. DeBerardinis, R. J., Lum, J. J., Hatzivassiliou, G. & Thompson, C. B. The biology of cancer: metabolic reprogramming fuels cell growth and proliferation. *Cell Metab.* **7,** 11–20 (2008).
4. Vander Heiden, M. G., Cantley, L. C. & Thompson, C. B. Understanding the Warburg effect: the metabolic requirements of cell proliferation. *Science* **324,** 1029–1033 (2009).
5. Berg, J. M., Tymoczko, J. L. & Stryer, L. *Biochemistry* 6th edn 577–589 (W. H. Freeman, 2006).
6. Vogelstein, B., Lane, D. & Levine, A. J. Surfing the p53 network. *Nature* **408,** 307–310 (2000).
7. Vousden, K. H. & Prives, C. Blinded by the light: the growing complexity of p53. *Cell* **137,** 413–431 (2009).
8. Kondoh, H. *et al.* Glycolytic enzymes can modulate cellular life span. *Cancer Res.* **65,** 177–185 (2005).
9. Matoba, S. *et al.* p53 regulates mitochondrial respiration. *Science* **312,** 1650–1653 (2006).
10. Vousden, K. H. & Ryan, K. M. p53 and metabolism. *Nat. Rev. Cancer* **9,** 691–700 (2009).
11. Bunz, F. *et al.* Requirement for p53 and p21 to sustain G2 arrest after DNA damage. *Science* **282,** 1497–1501 (1998).
12. Tseng, Y. H. *et al.* New role of bone morphogenetic protein 7 in brown adipogenesis and energy expenditure. *Nature* **454,** 1000–1004 (2008).
13. Komarov, P. G. *et al.* A chemical inhibitor of p53 that protects mice from the side effects of cancer therapy. *Science* **285,** 1733–1737 (1999).
14. Inga, A. & Resnick, M. A. Novel human p53 mutations that are toxic to yeast can enhance transactivation of specific promoters and reactivate tumor p53 mutants. *Oncogene* **20,** 3409–3419 (2001).
15. Freedman, D. A. & Levine, A. J. Nuclear export is required for degradation of endogenous p53 by MDM2 and human papillomavirus E6. *Mol. Cell Biol.* **18,** 7288–7293 (1998).
16. Stommel, J. M. *et al.* A leucine-rich nuclear export signal in the p53 tetramerization domain: Regulation of subcellular localization and p53 activity by NES masking. *EMBO J.* **18,** 1660–1672 (1999).
17. Yan, W. & Chen, X. Characterization of functional domains necessary for mutant p53 gain of function. *J. Biol. Chem.* **285,** 14229–14238 (2010).
18. Nikolova, P. V., Henckel, J., Lane, D. P. & Fersht, A. R. Semirational design of active tumor suppressor p53 DNA binding domain with enhanced stability. *Proc. Natl Acad. Sci. USA* **95,** 14675–14680 (1998).
19. Au, S. W., Gover, S., Lam, V. M. & Adams, M. J. Human glucose-6-phosphate dehydrogenase: The crystal structure reveals a structural NADP(+) molecule and provides insights into enzyme deficiency. *Structure* **8,** 293–303 (2000).
20. Roos, D. *et al.* Molecular basis and enzymatic properties of glucose 6-phosphate dehydrogenase volendam, leading to chronic nonspherocytic anemia, granulocyte dysfunction, and increased susceptibility to infections. *Blood* **94,** 2955–2962 (1999).
21. Green, D. R. & Kroemer, G. Cytoplasmic functions of the tumour suppressor p53. *Nature* **458,** 1127–1130 (2009).
22. Bensaad, K. *et al.* TIGAR, a p53-inducible regulator of glycolysis and apoptosis. *Cell* **126,** 107–120 (2006).

METHODS

Antibodies and reagents. Antibodies against the following proteins/epitopes were used with the sources and dilution ratios indicated in parentheses: GFP (Clontech; 1:4,000); p53 (DO-1, Oncogene, and Santa Cruz Biotechnology; 1:1,000); *S. cerevisiae* G6PD and Flag (M2) (Sigma); and human G6PD (Abcam; 1:4,000 and Sigma; 1:2,000). The following reagents were purchased from Sigma: Flag peptide, glutathione reductase, *L. mesenteroides* and *S. cerevisiae* G6PD proteins, DHEA, glucose-6-phosphate, 6-phosphogluconate, $NADP^+$, insulin, rosiglitazone, dexamethasone, isobutylmethylxanthine, doxorubicin and [2-^{13}C]glucose.

Plasmids. The DNA fragments corresponding to the full-length G6PD and p53 were amplified by polymerase chain reaction (PCR) from Marathon-Ready HeLa complementary DNA (Clontech), and cloned into p3 × Flag-Myc-CMV-24 (Sigma) and pEGFP-C1 (Clontech). The pGEX-2TK-p53 plasmid was provided by J. Kobarg (Centro de Biologia Molecular Estrutural, Laboratório Nacional de Luz Síncrotron, Brazil). p53 proteins tagged with a single Flag epitope were constructed in pRK5 (ref. 23). For expressing p53 in yeast, p53 was fused to the Gal4 DNA-binding domain in pGBKT7 and to the *E. coli* DNA binding protein LexA in pGlida (Clontech). For expressing p53 in bacteria, p53 was amino-terminally tagged with a Flag epitope in pET28(a). All deletion and point mutations were made by PCR and confirmed by DNA sequencing.

Analysis of the PPP and glycolysis in cells. The flux through the oxidative branch of the PPP and glycolysis was assessed with carbon-13 NMR spectrometry as described previously[24]. $p53^{+/+}$ and $p53^{-/-}$ HCT116 were cultured in triplicate 10 cm plates for three days to approximately 60–70% confluence. After being washed with medium containing no glucose, the cells were incubated with medium containing 10 mM [2-^{13}C]glucose for 9 h. The rates of total glucose consumption and lactate formation were determined with a bench-top analyser (Nova Biomedical). Incorporation of ^{13}C in carbon 2 and 3 of lactate results from glucose metabolism through glycolysis and oxidative PPP, respectively. To determine the incorporation of ^{13}C into lactate at these carbon positions, the final medium from each culture was analysed in a 20-mm NMR tube with a 9.4 T spectrometer (Varian) at 100.66 MHz. A 90° excitation pulse was applied every 6 s (fully relaxed), with broadband decoupling used only during ^{13}C data acquisition (no nuclear Overhauser effect enhancement). Spectra were acquired with 32,768 points, a spectral width of 25,000 Hz and 3,000 excitations. Free induction decays were apodized with exponential multiplication (1 Hz line broadening). The ratio of ^{13}C in carbons 2 (reflecting glycolytic flux) and 3 (reflecting oxidative PPP flux) of lactate and the rate of glucose consumption were used to estimate the oxidative PPP flux.

Glucose consumption and lactate production. Cells were seeded in culture plates and cultured for 6 h. The culture medium was then changed and cells were incubated for an additional 15 h. Glucose levels in the culture medium were measured using the Glucose (GO) Assay Kit (Sigma). Lactate levels were determined using a Lactate Assay Kit (Eton Bioscience).

Cell culture and gene knockdown with shRNA and siRNA. Cells were maintained in standard culture conditions. $p53^{-/-}$ and $p53^{+/+}$ MEF cells were established from embryos of the corresponding mice generated by crossing p53 heterozygote mice (B6.129S2-*Trp53tm1Tyj*/J, The Jackson Laboratory). *G6PD* siRNAs were purchased from Invitrogen (Catalogue No. HSS103891 and HSS103892). *G6PD* shRNAs were purchased from Open Biosystem. The target sequence for *G6PD* shRNA #1 (Catalogue No. RHS3979-9595543) is 5′-GTCGTCCTCTATGTGGAGAAT-3′, and the target sequence for *G6PD* shRNA #4 (Catalogue No. RHS3979-9595544) is 5′-CAACAGATACAAGAACGTGAA-3′. Expression plasmid for *p53* shRNA was made in a vector that co-expresses GFP (provided by D. C. Chan, California Institute of Technology, Pasadena, USA.). The targeted sequence for *p53* is: 5′-GACTCCAGTGGTAATCTAC-3′ (ref. 25). siRNAs and shRNA plasmids were transfected into cells using Lipofectamine 2000 (Invitrogen). Stable shRNA transfectants were selected in medium containing puromycin (1 μg ml^{-1}) and pooled after culturing for 3–4 weeks.

G6PD enzyme activity. G6PD enzyme activity was determined as described previously[26]. First, the combined activity of G6PD and 6-phosphogluconate dehydrogenase (6PGD), the second enzyme of the PPP, which also produces NADPH, was measured by the rate of conversion of $NADP^+$ to NADPH in the presence of glucose-6-phosphate (G6P). The activity of 6PGD alone was then measured by the conversion of $NADP^+$ to NADPH in the presence of 6-phosphogluconate (6PG). G6PD activity was calculated as the difference of these two activities. Cell lysates were added to the reaction buffer containing 50 mM Tris and 1 mM $MgCl_2$, pH 8.1. Substrate concentrations used were: G6P and 6PG (200 μM), and $NADP^+$ (100 μM). Enzyme activities were normalized on the basis of protein concentration, which was determined by a BCA Assay Kit (Pierce). The data are expressed in arbitrary absorption units.

Immunoprecipitation and indirect immunofluorescence. Immunoprecipitation was carried out as described previously[27]. Briefly, cell lysates were made by sonication in buffer containing 20 mM HEPES (pH 7.8), 400 mM KCl, 5% glycerol, 5 mM EDTA, 0.4% NP40 and protease inhibitors, and pre-cleared by centrifugation. The supernatants were then diluted in 20 mM HEPES (pH 7.8), 50 mM KCl, 5% glycerol, 2.5 mM $MgCl_2$, 0.05% NP40 and incubated with indicated protein A/G-Sepharose-bound antibodies for 4 h at 4 °C. Beads were pre-blocked with 2% BSA in PBS and 0.05% 3-[(3-cholamidopropyl)-dimethylammonio]-1-propane sulphonate (CHAPS) before immunoprecipitation. After incubation, beads were washed twice with lysis buffer, four times with ice-cold PBS and boiled in 2× loading buffer. Protein samples were resolved by SDS–PAGE.

The indirect immunofluorescence was carried out as described previously[23,28]. Briefly, cells cultured on coverslips were treated separately with dimethylsulphoxide (DMSO) and etoposide (20 μM) for 24 h. Cells were fixed in 4% paraformaldehyde for 10 min, permeabilized with 0.1% Triton X-100 for 5 min, blocked with 5% BSA and incubated with antibodies as indicated, followed by a Texas-red-conjugated anti-rabbit IgG and a fluorescein isothiocyanate (FITC)-conjugated anti-mouse IgG antibody. The cells were mounted with 4,6-diamidino-2-phenylindole (DAPI)-containing medium (Vector Laboratories) and the images were acquired with a confocal microscope.

Protein purification. Flag-tagged G6PD and p53 were expressed in H1299 cells or 293T cells. When indicated, cell lysates were separated into cytosolic and nuclear fractions. Proteins were purified using M2 beads, as previously described[23,29]. For purifying Flag–G6PD, 10 μM $NADP^+$ was included in the lysis buffer. Glutathione *S*-transferase (GST)–p53 was expressed in DH5α cells after induction with 2 mM isopropyl-β-D-thiogalactoside (IPTG) at 37 °C, and purified by glutathione beads (Amersham Biosciences).

Surface plasmon resonance analysis of p53–G6PD interaction. Surface plasmon resonance analysis was carried out at 25 °C with a Pharmacia Biosensor BiAcore 3,000 instrument (BiAcore) according to the manufacturer's instructions. *S. cerevisiae* G6PD was immobilized on the surface of a CM5 sensor chip in 10 mM sodium acetate buffer (pH 4.5) and resulted in 8,000 response units. A reference surface was used as a blank to correct for instrumental and buffer effects without protein injection. The amount of protein bound to the sensor chip was monitored by the change in refractive index. Purified Flag–p53 was diluted, and run across each sensor surface at five different concentrations in a running buffer of PBS at a flow rate of 30 μl min^{-1}. Flag–p53 protein concentrations were 0.03–0.9 μM. Dissociation constants from five serial dilutions of each protein and other kinetic parameters were calculated using the BIA Evaluation software.

NADPH level. NADPH levels were determined as described previously[30]. Cell lysates were prepared in buffer containing 0.1 M Tris-HCl, pH 8.0, 0.01 M EDTA and 0.05% (v/v) Triton X-100, sonicated and centrifuged at (2,400*g*) at 4 °C. The total levels of NADPH plus reduced nicotinamide adenine dinucleotide (NADH) in the lysates were assayed by spectrometry (Beckman DU 640 spectrophotometer, Beckman Coulter) at a wavelength of 341 nm. The levels of NADPH in the lysates were determined on the basis of the decrease in absorbance at 341 nm after NADH was converted to nicotinamide adenine dinucleotide (NAD) by glutathione reductase.

Lipid synthesis. Lipid accumulation was measured using Oil Red O staining, as described previously[12]. Briefly, cells were grown in medium supplemented with insulin (2 μM), dexamethasone (1 μM) and isobutylmethylxanthine (0.25 mM) for 2 d, and in medium supplemented with insulin and rosiglitazone (10^{-7} M) for an additional 5 d. The medium was changed every other day. Cells were then fixed with 10% buffered formalin for 16 h at 4 °C and were stained with a filtered Oil Red O solution (0.5% Oil red O in isopropyl alcohol) for 2 h at room temperature.

Analysis of $p53^{+/+}$ and $p53^{-/-}$ mice. Four-week-old $p53^{+/+}$ and $p53^{-/-}$ mice (B6.129S2-*Trp53tm1Tyj*/J) were obtained from the Model Animal Research Center (Nanjing University, China) and were maintained on a regular diet. Tissues were excised for the measurement of the G6PD activity and NADPH level. Liver tissues were fixed in 10% formalin and paraffin-embedded. Sections were prepared and stained with haematoxylin and eosin. All animal experiments were carried out in accordance with the local Animal Care and Use Committee.

Statistical analysis. Statistical significance was analysed by Student's *t*-test and expressed as a *P* value.

23. Tang, J. *et al.* Critical role for Daxx in regulating Mdm2. *Nat. Cell Biol.* **8,** 855–862 (2006).
24. Mancuso, A., Sharfstein, S. T., Tucker, S. N., Clark, D. S. & Blanch, H. W. Examination of primary metabolic pathways in a murine hybridoma with carbon-13 nuclear magnetic resonance spectroscopy. *Biotechnol. Bioeng.* **44,** 563–585 (1994).

DOI: 10.1038/ncb2172

25. Brummelkamp, T. R., Bernards, R. & Agami, R. A system for stable expression of short interfering RNAs in mammalian cells. *Science* **296,** 550–553 (2002).
26. Tian, W. N. *et al.* Importance of glucose-6-phosphate dehydrogenase activity for cell growth. *J. Biol. Chem.* **273,** 10609–10617 (1998).
27. Adorno, M. *et al.* A mutant-p53/Smad complex opposes p63 to empower TGF β-induced metastasis. *Cell* **137,** 87–98 (2009).
28. Du, W. *et al.* Suppression of p53 activity by Siva1. *Cell Death Differ.* **16,** 1493–1504 (2009).
29. Tang, J. *et al.* A novel transcription regulatory complex containing death domain-associated protein and the ATR-X syndrome protein. *J. Biol. Chem.* **279,** 20369–20377 (2004).
30. Zhang, Z., Yu, J. & Stanton, R. C. A method for determination of pyridine nucleotides using a single extract. *Anal. Biochem.* **285,** 163–167 (2000).

nature cell biology

DOI: 10.1038/ncb2172

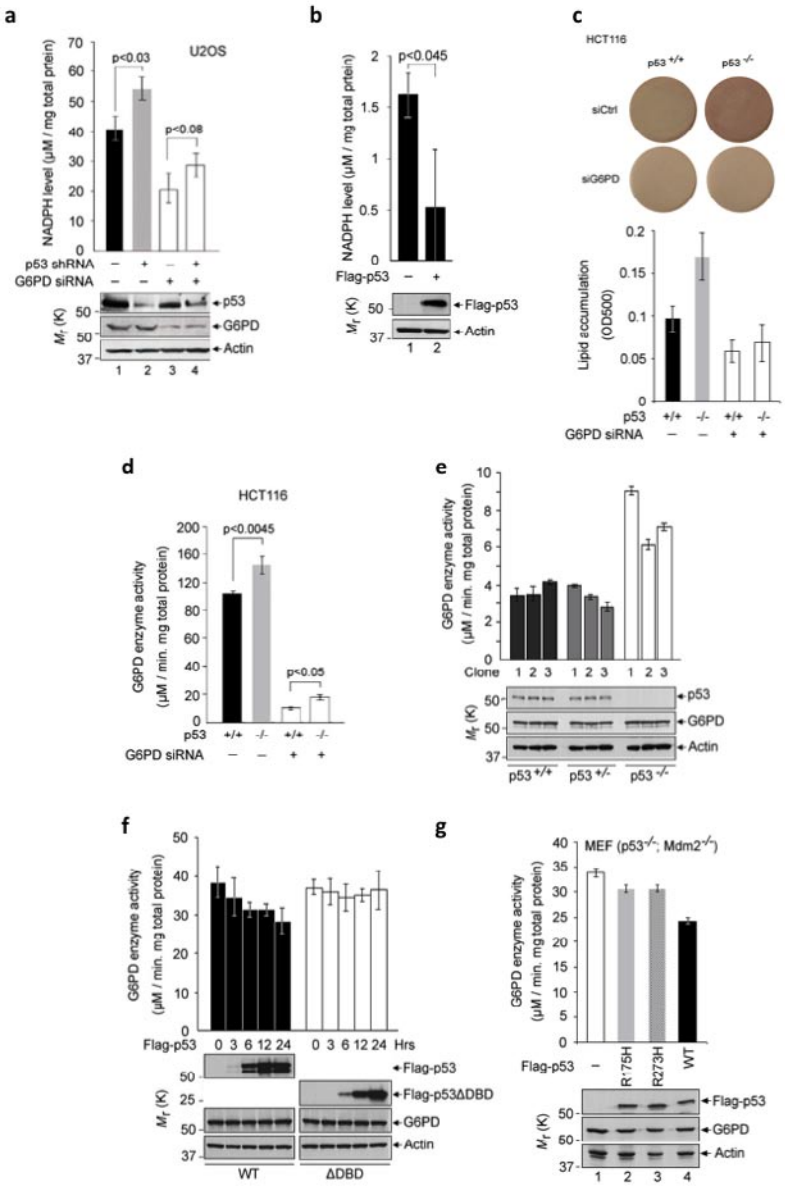

Figure S1 p53 regulates cellular NADPH and lipid levels via inhibition of G6PD. (**a**) U2OS cells stably expressing p53 shRNA or a control shRNA were transfected with control siRNA or G6PD siRNA. NADPH levels and protein expression are shown. Data are means ± S.D. (n=3). (**b**) NADPH levels (means ± S.D., n=3) in H1299 cells transfected with Flag-p53 or the vector control (-). (**c**) Lipid accumulation in *p53*$^{+/+}$ and *p53*$^{-/-}$ HCT116 cells treated with G6PD siRNA or control siRNA. Cells were cultured in medium containing insulin, rosiglitazone, isobutylmethylxanthine (IBMX), and dexamethasone for 7 days. Lipid contents were analyzed by Oil Red O staining. Data are means ± S.D. (n=3). (**d**) *p53*$^{+/+}$ and *p53*$^{-/-}$ HCT116 cells transfected with G6PD siRNA or control siRNA (Fig. 1b) were assayed for G6PD activity. Data are means ± S.D. (n=3). p value are shown. (**e**) Top: G6PD activity (means ± S.D., n=3) from three different clones each of *p53*$^{+/+}$, *p53*$^{+/-}$, and *p53*$^{-/-}$ MEFs. Bottom: G6PD and p53 levels. (**f**) H1299 cells were transfected with Flag-p53/pRK5 or Flag-p53ΔDBD/pRK5. G6PD activity (top, means ± S.D., n=3) and protein expression (bottom) were determined at the indicated times after transfection. (**g**) G6PD activity (means ± S.D., n=3) in *p53*$^{-/-}$ *Mdm2*$^{-/-}$ MEF cells transfected separately with wild type p53 and each of the mutant p53. Protein expression is shown below.

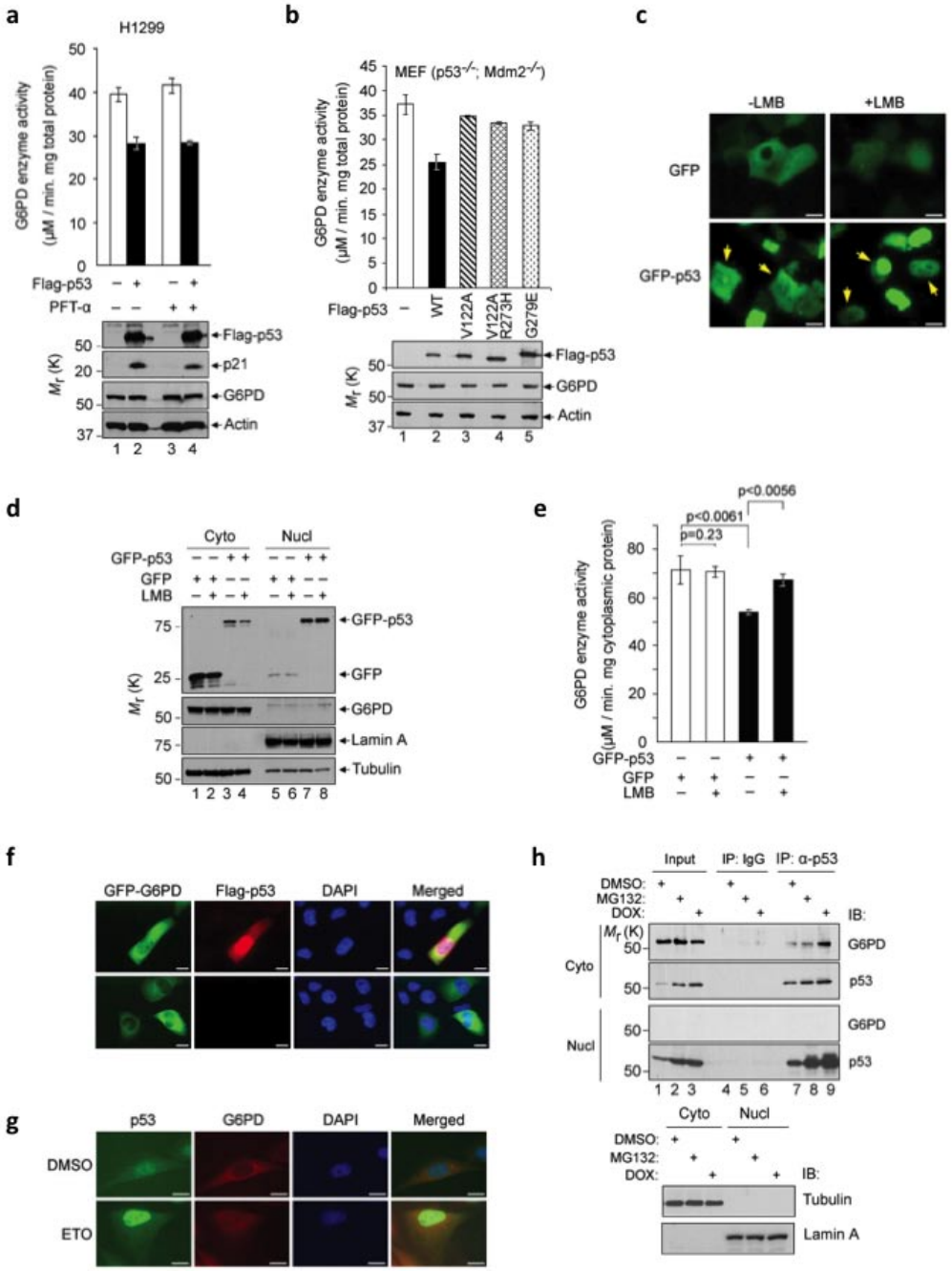

Figure S2 Cytosolic p53 inhibits G6PD. (**a**) p53 inhibits G6PD independently of transcription. H1299 cells transfected with Flag-p53 or control vector were treated with 20 μM PFTα for 24 h. G6PD activity and protein expression are shown. Data are means ± S.D. (n=3). (**b**) G6PD activity (means ± S.D., n=3) in *p53*$^{-/-}$ *Mdm2*$^{-/-}$ MEF cells transfected separately with wild type p53 and each of the mutant p53. Protein expression is shown below. (**c-e**) p53 inhibition of G6PD activity requires its cytosolic localization. H1299 cells expressing GFP or GFP-p53 were treated with LMB (1 μM) for 6 h. Transfected cells were visualized by microscope (**c**). Scale bars, 10μm. Yellow arrows indicated the different localization of GFP-p53 with and without LMB treatment. Cell extracts were separated into nuclear and cytoplasmic fractions, and each was analyzed by western blotting (**d**). G6PD activity in the cytoplasmic fractions was measured (**e**). Data in **e** are means ± S.D. (n=3). (**f**) Co-localization of transfected p53 and G6PD in the cytosol. H1299 cells were transfected with GFP-G6PD together with Flag-p53 or a control vector. Flag-p53 was immuno-stained with an anti-Flag antibody followed by a Texas Red-conjugated secondary antibody, and DNA was stained with DAPI. The individual and merged images are shown. Scale bars, 10μm. (**g**) Co-localization of endogenous p53 and G6PD in the cytosol. U2OS cells were treated with etoposide (ETO, 20 mM) or vehicle (DMSO) for 24 h. Endogenous p53 was detected by a mouse anti-p53 antibody followed by a FITC-conjugated secondary antibody, and G6PD by a rabbit anti-G6PD antibody followed by a Texas Red-conjugated secondary antibody. Scale bars, 10μm. (**h**) Lysates from *p53*$^{+/+}$ HCT116 cells treated with MG132 (20 μM), Dox (2 μM), or vehicle (DMSO) were separated into cytosolic (Cyto) and nuclear (Nucl) fractions. Each fraction was immunoprecipitated with anti-p53 antibody or a control antibody (IgG). Top: inputs and immunoprecipitated proteins (IP) were analyzed by western blotting using antibodies for G6PD and p53. Bottom: tubulin and lamin A in the lysates were analyzed as controls for fractionation and sample loading.

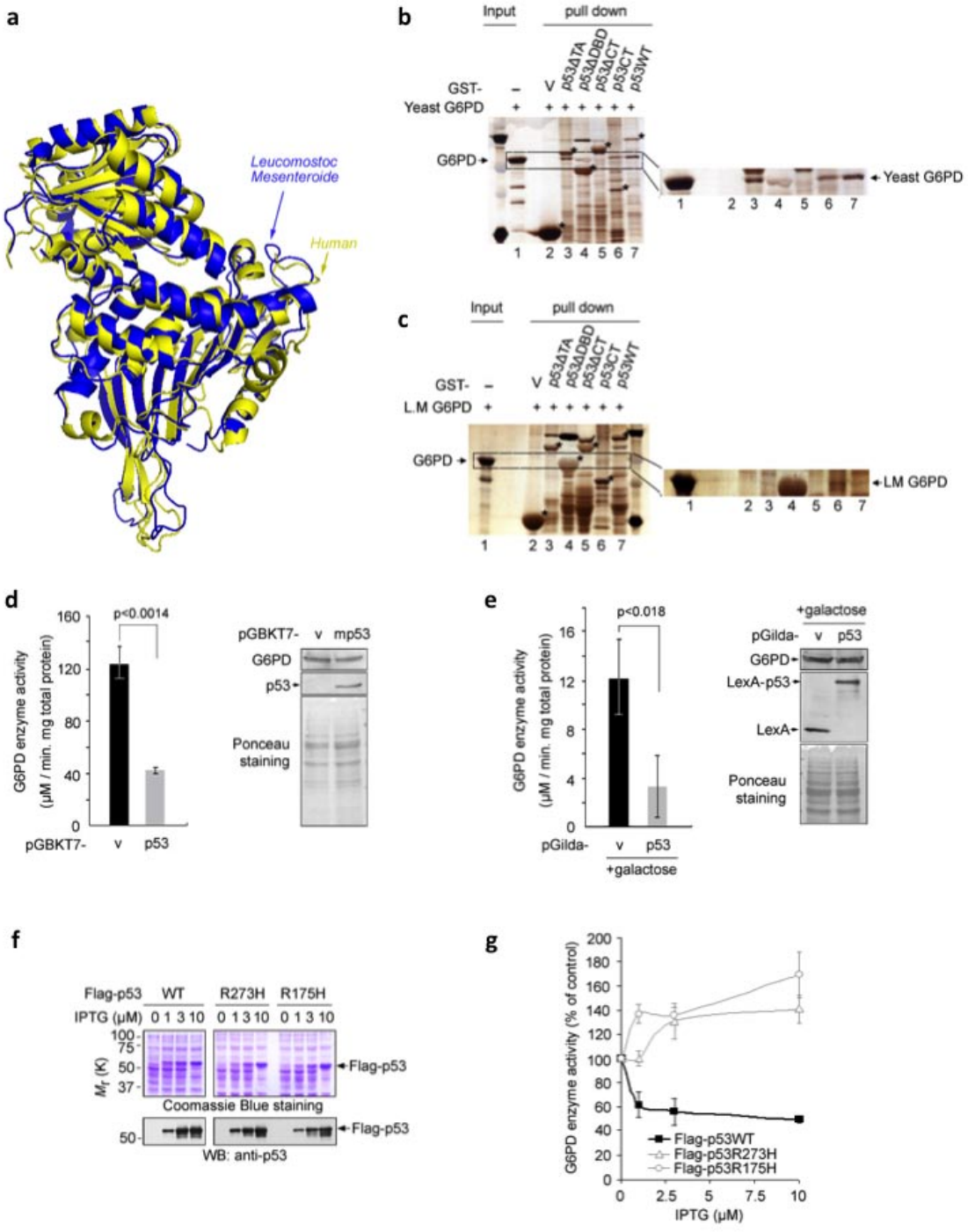

Figure S3 p53 interacts with and inhibits yeast and bacterial G6PD proteins. (**a**) Comparison of the three-dimensional structure of the human G6PD (PDB entry: 2BH9) (yellow) to that of *L. mesenteroides* G6PD (PDB entry: 1DPG) (blue). This figure was produced with PyMOL (W. L. DeLano (2002) PyMOL, DeLano Scientific, San Carlos, CA). (**b, c**) Human p53 interacts with yeast and bacterial G6PD proteins. GST fusion of p53 and p53 mutants immobilized on beads were incubated with G6PD from *S. cerevisiae* (**c**) and *L. mesenteroides* (**b**). Beads-bound proteins were analyzed with SDS-PAGE and silver staining. Asterisk indicates the localization of the GST-p53 proteins. (**d, e**) Yeast AH109 cells were transformed with either pGBKT7 (parental vector) or pGBKT7 expressing mouse p53. The transformants were grown in medium with 2% glucose (**d**). Yeast EGY48 cells were transformed with either pGilda (parental plasmid that expressed the bacterial DNA binding protein LexA) or pGilda expressing LexA fusion of human p53. The transformants were grown in medium with 2% galactose for 2 h before harvest (**e**). Left: G6PD activity in the transformants. Right: cell lysates were resolved on SDS-PAGE and analyzed by western blot (top and middle) and Ponceau S staining (bottom). Data are means ± S.D. (n=3). (**f, g**) Expression of wild type and mutant p53 in *E. coli* was induced by increasing amounts of IPTG. Protein expression (examined by Coomassie blue staining, **f**) and G6PD activity (**g**) are shown. Data in **g** are means ± S.D. (n=3).

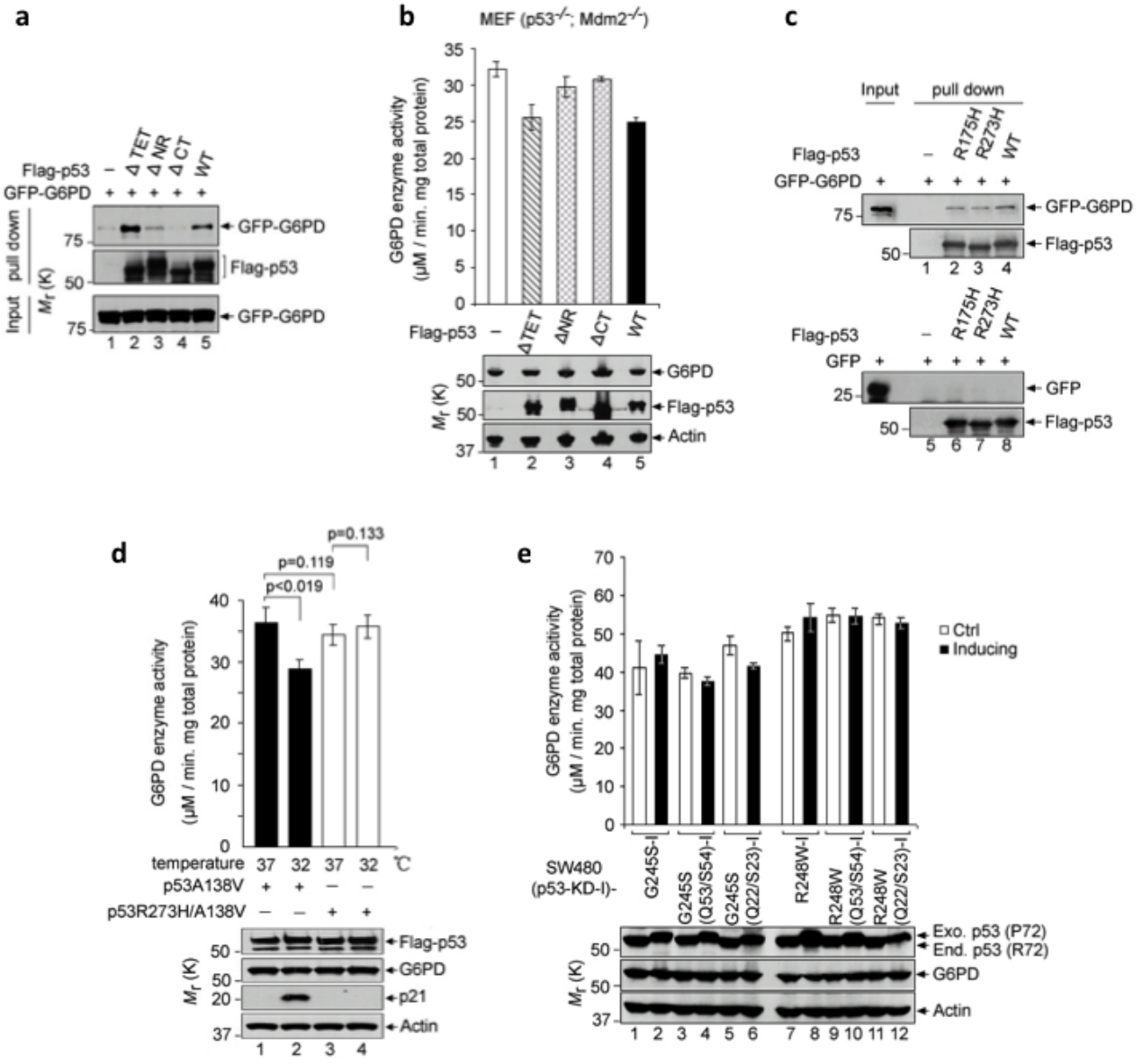

Figure S4 Wild type p53, but not tumor-associated p53 mutants, regulates G6PD activity. (**a**, **c**) Lysates from *p53*$^{-/-}$*Mdm2*$^{-/-}$ MEF cells transfected with GFP (**c**) or GFP-G6PD (**a**, **c**) were incubated with control beads and Flag-tagged p53 and p53 mutants immobilized on M2 beads. The beads-bound (pull down) proteins and input were analyzed by Western blot. (**b**) G6PD activity (means ± S.D., n=3) in *p53*$^{-/-}$ *Mdm2*$^{-/-}$ MEF cells transfected separately with wild type and mutant p53. (**d**) G6PD activity (means ± S.D., n=3) in H1299 cells that were transfected with p53 A138V or A138V/R273H mutant and cultured at 32 or 37 °C. (**e**) SW480 cell lines were treated with vehicle (Ctrl), or with 0.5 μg/ml Doxycycline for 3 days to simultaneously induce knockdown of endogenous p53 mutant by shRNA and expression of exogenous p53 mutants. G6PD activity (top) and protein expression (bottom) were analyzed. The endogenous (End.) p53 mutant contains Arg at position 72, while exogenous (Exo.) p53 mutants have Pro at this position. Consequently, endogenous and exogenous p53 proteins migrated differently on SDS-PAGE. The exogenous p53 mutants were resistant to shRNA and have either the conformation mutation G245S or the contact mutation R248W, each alone (G245S-I and R248W-I) or in combination with mutations (Q22/S23) in the activation domain (AD) 1 (G245S(Q22/S23)-I and R248W(Q22/S23)-I) or mutations (Q53/S54) in AD2 (G245S(Q53/S54)-I and R248W(Q53/S54)-I) [10]. Data are means ± S.D. (n=3).

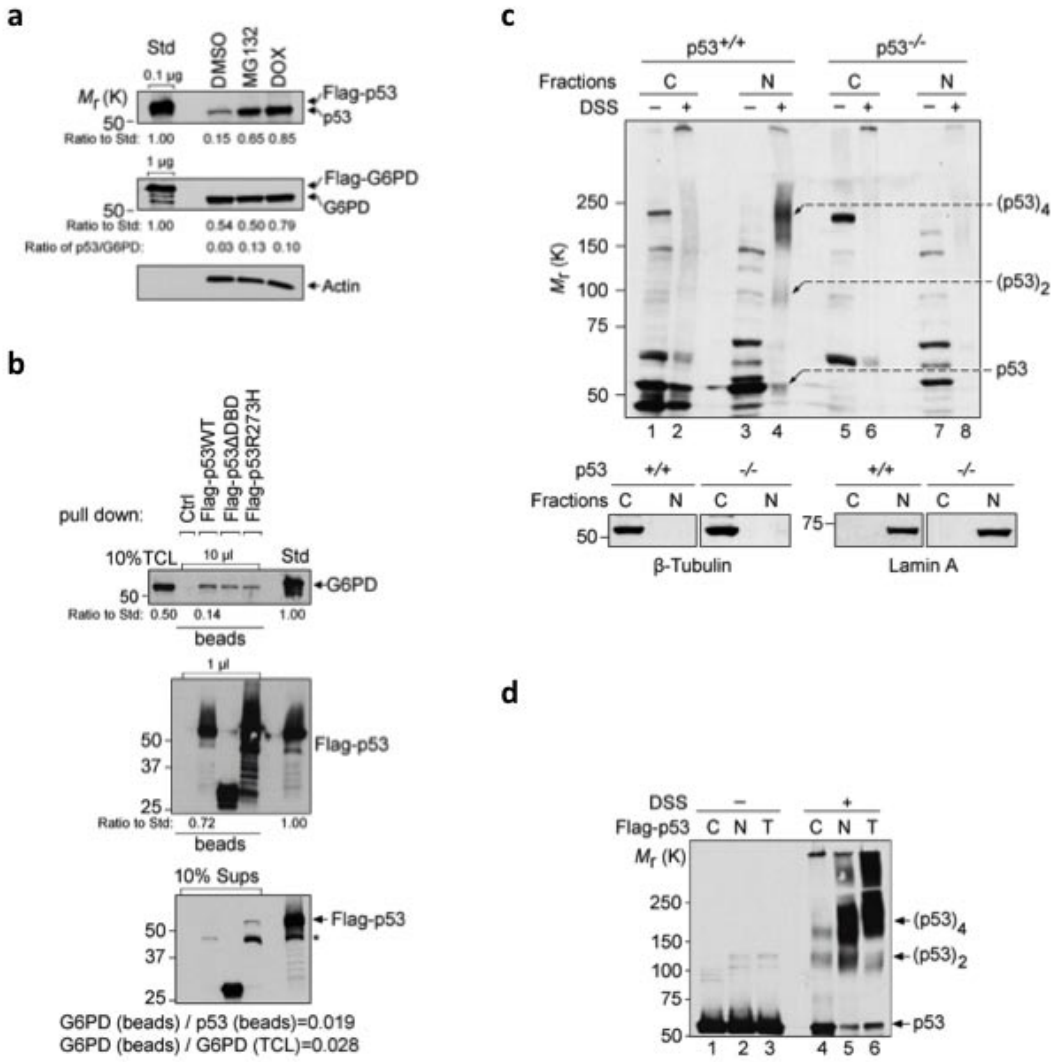

Figure S5 Evidence that p53 inhibits G6PD through a catalytic action and that cytosolic p53 is intrinsically different from nuclear p53. (**a**) *p53*$^{+/+}$ HCT116 cells were treated with MG132, DOX, or vehicle (DMSO). Cytosolic fraction was analyzed for p53 and G6PD expression along with the indicated amounts of purified Flag-p53 and Flag-G6PD protein standards by western blot. Protein bands were qualified by NIH Image software, and the ratios of p53 and G6PD in the extracts to the corresponding standards were calculated. Based on these ratios and the relative amounts of the p53 and G6PD protein standards, the p53/G6PD ratios in the cell lysates are calculated. (**b**) Lysates from *p53*$^{-/-}$ MEF cells were first incubated with Flag-tagged p53 proteins immobilized on beads and control beads, and then were separated from the beads (Figs. 5c, d). G6PD in the total cell lysates (TCL) (top panel), beads-bound G6PD and p53 proteins (top and middle panels), and p53 proteins in the extracts after bead-binding (Sups) (bottom panels) were analyzed by western blot along with the same amount of purified G6PD and p53 protein standards (Std). Shown at the bottom are the ratios of beads-bound G6PD versus p53, of G6PD on beads versus G6PD in total cell lysates, and of p53 versus G6PD in the Sups after binding. Note that amounts of G6PD stably associated with immobilized p53 were minimal, while the amounts of wild type p53 released from beads were below detection. Asterisk indicates a non-specific band. (**c**) Cytosolic and nuclear fractions of *p53*$^{+/+}$ and *p53*$^{-/-}$ HCT116 cells were treated with and without the chemical cross-linker DSS. Cell lysates were analyzed with western blot. Tubulin and LaminA in untreated lysates were analyzed as controls for fractionation and sample loading. p53 monomer, dimer, and tetramer are indicated. (**d**) Flag-p53 purified from cytosolic (C), nuclear (N), and total (T) lysate fractions (Fig. 5g) was treated with or without DSS, and examined by western blot.

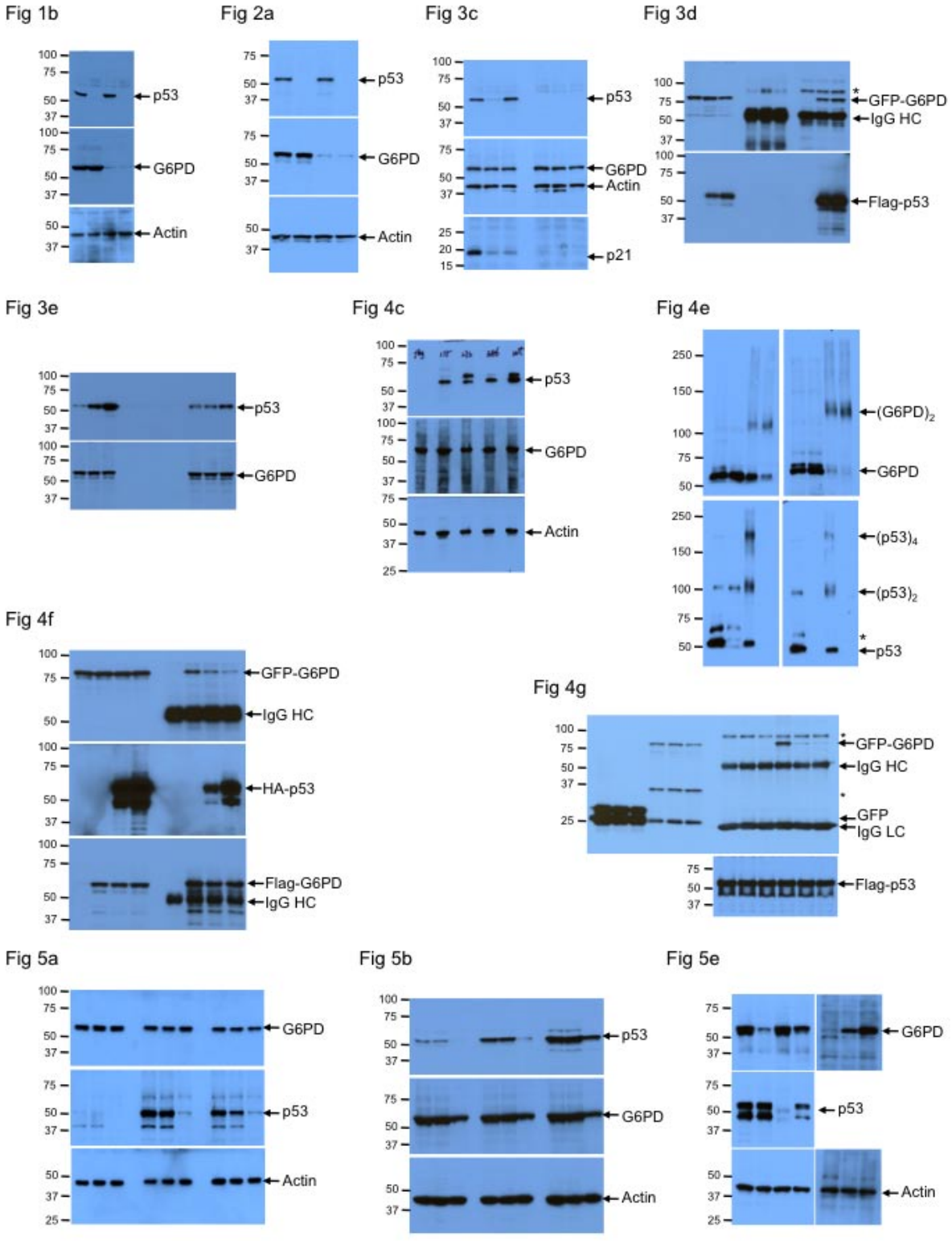

Figure S6 Full scans of western data. *Non-specific bands